Hindawi
Advances in Meteorology
Volume 2022, Article ID 7351150, 15 pages
https://doi.org/10.1155/2022/7351150

Research Article

Parameter Sensitivity Analysis and Optimization of the Single-Layer Urban Canopy Model in the Megacity of Shanghai

Xiangyu Ao [1,2,3] **and Ning Zhang** [4]

[1]*Shanghai Typhoon Institute and Key Laboratory of Numerical Modeling for Tropical Cyclone of the China Meteorological Administration, Shanghai 200030, China*
[2]*Shanghai Key Laboratory of Meteorology and Health, Shanghai 200030, China*
[3]*Key Laboratory of Cities Mitigation and Adaptation to Climate Change, Shanghai, China Meteorological Administration, Shanghai 200030, China*
[4]*School of Atmospheric Sciences, Nanjing University, Nanjing 210023, China*

Correspondence should be addressed to Ning Zhang; ningzhang@nju.edu.cn

Received 28 December 2021; Revised 19 March 2022; Accepted 25 March 2022; Published 11 April 2022

Academic Editor: Stefania Bonafoni

In order to meet the demand of more refined urban weather forecast, it is of great practical significance to improve and optimize the single-layer urban canopy model (SLUCM) suitable for the megacity of Shanghai. In this paper, based on the offline SLUCM model driven by a whole-year surface flux observation data in the Shanghai central business district, a series of parameter sensitivity tests are carried out by using the one at a time (OAT) method, the relative importance and a set of optimized parameters of the SLUCM suitable for high-density urban area are established, and the improvement of simulation is evaluated. The results show that SLUCM well reproduces the seasonal mean diurnal patterns of the net all-wave radiation flux (Q^*) and sensible heat flux (Q_H) but underestimates their magnitudes. Both Q^* and Q_H are linearly sensitive to the albedo, and most sensitive to the roof albedo, the second to the wall albedo, but relatively insensitive to the road albedo. The sensitivity of Q^* and Q_H to emissivity is not as strong as that of albedo, and the variation trend is also linear. Similar to albedo, Q^* and Q_H are most sensitive to roof emissivity. The effect of thermal parameters (heat capacity and conductivity) on fluxes is logarithmic. The sensitivity of surface fluxes to geometric parameters has no specific variation pattern. After parameter optimization, RMSE of Q^* decreases by about 3.4–18.7 Wm^{-2} in four seasons. RMSE of the longwave radiation ($L_\uparrow$) decreases by about 1.2–7.87 Wm^{-2}. RMSE of Q_H decreases by about 2–5 Wm^{-2}. This study provides guidance for future development of the urban canopy model parameterizations and urban climate risk response.

1. Introduction

Since the reform and opening up in 1978, China has experienced more rapid urbanization rate than the average level of the world and Asia. Megacities are mainly characterized by dense population and high-rise buildings. Tremendous land use and land cover changes in urban areas have formed unique urban climatic characteristics, such as urban heat island and urban dry island [1–5]. The fundamental cause for these urban climate effects is that the modification of the underlying surface changes the original energy and mass exchange process between the surface and the atmosphere, finally resulting in the weather and climate change [6–8]. An in-depth understanding of the energy and mass exchanges between urban surface and atmosphere is of great significance to the mechanism of the formation of urban heat island and the difference of boundary layer structures between urban and rural areas. At the same time, it also provides a reliable basis for the establishment of the urban land surface parameterization scheme [9, 10].

With the enrichment of computing resources, the resolution of numerical weather prediction (NWP) models has been improved to the kilometer level. It is of great necessity to couple a more refined and independent urban land

surface model in mesoscale or regional NWP models [11–14]. From the morphological point of view, urban land surface models mainly include three types: the first type is the slab model; that is, the energy flux between the surface and the atmosphere is estimated by setting a series of urban surface parameters to characterize the underlying urban surface. The advantage of this kind of model is that it needs fewer forcing variables, all of which are conventional meteorological observation data, and the calculation method is relatively simple. The disadvantage is that it does not consider the three-dimensional urban structure [15, 16]. The second type is the single-layer urban canopy model (SLUCM) [17]. SLUCM distinguishes different effects of three urban facets: roof, wall, and road. The urban street canyon is two-dimensional (2D), but the radiation treatment is three-dimensional (3D), which considers different street canyon directions and daily changes of solar azimuth. In the SLUCM, the exchange and feedback between the urban surface and the atmosphere only occur above the urban canopy top (roof level). The air within the urban canyon is regarded as a homogeneous medium, so only one single point air is used to represent the temperature and humidity state within the urban canyon. The third type is the multilayer urban canopy model (MLUCM) [18, 19]. Based on SLUCM, the urban canopy is further divided into multiple layers. Considering the interaction between layers, the turbulent exchange processes within the urban canyon and below the urban roughness sublayer can be simulated for MLUCM. Although the MLUCM can simulate the heat, water, and momentum exchanges within the urban canyon in more detail, it requires larger computational resources than the SLUCM. The single-layer urban canopy model (SLUCM) is of medium simplicity and more efficient and is easy to be coupled with mesoscale weather prediction models [20] such as WRF (weather research and forecasting model). It has been developed rapidly and used more widely in the last two decades [21–23]. The bottleneck for SLUCM is that it has relatively poor representation for urban hydrological processes. Efforts have been made to include more detailed representation of urban hydrological or evaporative processes by introducing vegetation surfaces or irrigation in the SLUCM [24–26]. However, these efforts also introduce additional input parameters that bring uncertainty to SLUCM.

The SLUCM requires many input parameters, among which the meteorological forcing input parameters such as air temperature, wind speed, humidity, surface pressure, and solar radiation can be obtained directly through observations or NWP models. However, other surface thermal parameters such as heat capacity, conductivity, emissivity, albedo, and morphological parameters cannot easily obtain accurate values, which brings great uncertainty to the model. The parameter sensitivity study conducted by [27] for several urban canopy models with different complexity over the urban area of Singapore suggests that the uncertainty of model parameters even plays a more dominant role in the model error statistics than the choice of model, which significantly indicates the importance of model parameter value settings. Therefore, the parameter sensitivity analysis of urban land surface models to determine the reasonable range of parameter values and the relative importance of each parameter is very important before coupling into mesoscale and even global numerical models. Previous scholars have carried out simulation and parameter sensitivity tests for the SLUCM using observational data of Vancouver, Princeton, Marseille, and Nanjing [11, 28–30]. Due to the heterogeneity and complexity of urban surfaces, the interaction between urban underlying surface and atmosphere is unique in each city. However, most of the current urban canopy simulation studies do not locally optimize the model parameters based on energy flux measurements and thus fail to fully reflect the advantages of urban canopy models compared with traditional slab models. Previous studies mainly evaluate sites located at low-density or residential areas with short periods (i.e., a few days), and parameter sensitivity studies of SLUCM have not been conducted yet at high-rise commercial sites with long periods (i.e., one year or longer). As the largest city in China, the underlying surface of Shanghai is much more heterogeneous than other relatively small and medium-size cities. The parameter sensitivity analysis and optimization of SLUCM in Shanghai will help improve the finer-scale weather forecast ability of NWP models and the ability of urban disaster prevention and reduction. This paper will evaluate the applicability of the SLUCM which is widely applied in the mesoscale WRF model using a full-year measurements of surface radiation, energy fluxes, and conventional meteorological variables in central Shanghai. It will also give an optimized parameter set of the SLUCM which is more suitable for the Shanghai megacity. This work is also an early-stage preparation for implementing the SLUCM in the 9 km (3 km) resolution operational numerical weather prediction system at the Shanghai Meteorological Service [31].

2. Data and Methodology

2.1. Description of Measurement Data. The surface flux measurement site (Xujiahui, hereafter XJH site) for model evaluation is located on the roof tower of the new building of Shanghai Meteorological Service (31.19°N, 121.43°E). The building height is about 55 m and the tower height is about 25 m; hence, the total height of instruments is about 80 m above the ground level. The XJH site is a typical densely built-up central urban site. Based on the GIS survey [16], the average building height within 500 m around the site is about 35.9 m and the urban coverage ratio is quite high ($f_{\mathrm{urb}} = 0.86$). The raw turbulence data are carefully quality controlled, and fluxes are computed by eddy covariance method at 30 min intervals. Details can be seen in [32]. A full-year data from December 2012 to November 2013 is used to drive and evaluate the SLUCM.

Figure 1 shows the seasonal mean diurnal variation of meteorological input variables used for SLUCM offline evaluation. It can be seen that the downward shortwave radiation flux is the largest in spring and summer with

comparable peak values around 600 W m^{-2} at noon, followed by autumn, and the smallest in winter. The peaks are about 470 and 340 W m^{-2}, respectively. The downward longwave radiation flux is the largest in summer, followed by spring and autumn, and the smallest in winter. The seasonal variation characteristic for the downward longwave radiation flux corresponds well with the 2 m air temperature. The difference of the 10 m wind speed among each season is small, with the seasonal average diurnal variation range within 1.5–3 m s^{-1} with daily maximum occurrence in the afternoon, which is related to the reduction of wind speed caused by the blocking effect of tall buildings in this central business district. The relative humidity in summer and winter is greater than that in spring and autumn, with magnitudes of 50%–90%. The main feature of precipitation is that there is a precipitation peak from afternoon to evening (16:00–17:00 LST) in summer and autumn, corresponding to the frequent afternoon convection in summer and autumn, while the precipitation is strong at around 3:00–5:00 a.m. in winter and spring.

2.2. Overview of the Single-Layer Urban Canopy Model (SLUCM). The SLUCM model [17, 33] mainly simulates the upward radiation and turbulent heat fluxes between the near surface and the atmosphere as the lower boundary layer condition for mesoscale numerical models (Figure 2). When SLUCM is coupled to atmospheric models, its horizontal dimension is a model grid, and its vertical dimension is the height from the surface to the bottom layer of the atmospheric models. It considers the trapping effect of 3D urban street canyons on radiation, building heat storage, and turbulence enhanced by large urban roughness. It describes the urban geometry, roughness, radiation, and thermal properties by giving a series of parameters. There are three urban categories (low-intensity residential, high-intensity residential, and commercial area) with different input parameter values. The open source version v3.4.1 of SLUCM (https://ral.ucar.edu/solutions/products/unified-noah-lsm) is used to carry out parameter sensitivity tests and optimization.

The basic unit of SLUCM is the 2D canyon structure (Figure 2), which is mainly determined by the building height, width, and roof width on a local scale. Three types of facets of SLUCM are normalized (W_{roof} + W_{road}: sum of roof and road width) as follows:

$$\begin{aligned} Z_{norm} &= \frac{Z_R}{\left(W_{roof} + W_{road}\right)}, \\ F_{walls} &= 2Z_{norm} = \frac{2Z_R}{\left(W_{roof} + W_{road}\right)}, \\ F_{roof} &= \frac{W_{roof}}{\left(W_{roof} + W_{road}\right)}, \\ F_{road} &= \frac{W_{roa\,d}}{\left(W_{roof} + W_{road}\right)}. \end{aligned} \tag{1}$$

Here, Z_R is the average building height (m), W_{roof} is the roof width (m), W_{road} is the road width (m), Z_{norm} is the normalized building height, and F_{walls}, F_{roof}, and F_{road} are the normalized wall, roof, and road ratio. The simulated fluxes (W m^{-2}) are weighted by these three normalized facets:

$$Q_{SLUCM} = F_{roof}Q_{roof} + F_{walls}Q_{walls} + F_{road}Q_{road}. \tag{2}$$

The equation for the net all-wave radiation flux (Q^*) is

$$Q^* = K_{\downarrow} - K_{\uparrow} + L_{\downarrow} - L_{\uparrow}, \tag{3}$$

where $K_{\downarrow}$, $K_{\uparrow}$, $L_{\downarrow}$, and $L_{\uparrow}$ are downward and upward shortwave and longwave radiation fluxes (W m^{-2}), respectively. The calculation of upward shortwave radiation ($K_{\uparrow}$) mainly considers the albedo of each surface, the sky view factor of wall and road, and the building shadow effect. The surface upward longwave radiation ($L_{\uparrow}$) is considered as a function of emissivity of each surface type and surface temperature.

The simulation of the surface sensible heat ($Q_{\mathrm{H\text{-}S}}$) and latent heat ($Q_{\mathrm{E\text{-}S}}$) flux is as follows:

$$\begin{aligned} Q_{\mathrm{H-S}} &= \rho\, c_{\mathrm{p}}\, C_{\mathrm{H}}\, U_{\mathrm{A}} \left(T_{\mathrm{S}} - T_{\mathrm{A}}\right), \\ Q_{\mathrm{E-S}} &= \rho\, L_{\mathrm{V}}\, C_{\mathrm{E}}\, U_{\mathrm{A}} \left(q_{\mathrm{S}} - q_{\mathrm{A}}\right). \end{aligned} \tag{4}$$

S represents the underlying natural surface, roof, or canyon space; A represents the atmosphere. ρ is the air density (kg m^{-3}), c_p is the specific heat of air (J kg^{-1} K^{-1}), and L_V is the latent heat of vaporization (J kg^{-1}). The turbulent heat and moisture exchange coefficients C_{H} and C_{E} are calculated by Monin-Obukhov similarity theory and are assumed identical in SLUCM. U_{A}, T_{A}, and q_{A} are wind speed (m s^{-1}), air temperature (°C), and specific humidity (kg kg^{-1}) at the forcing level, respectively. T_{s} and q_{s} are the surface temperature and specific humidity, respectively.

The calculation of surface dynamic roughness and zero plane displacement height of the urban canyon and roof has been changed from the earliest version as input parameters to the later geometric morphology method [30], which reduces the number of input parameters required by the model and is more scientific. The MacDonald method (1998) [34] takes into account the influence of building height variability on roof roughness by introducing the standard deviation of building height. In many studies, the variability of building height is considered as the dominant factor affecting the turbulence above the urban canopy.

There are many difficulties for the direct online evaluation of SLUCM coupled to mesoscale numerical models. For instance, the surface radiation bias from NWP models will directly affect the simulation ability of SLUCM for surface energy balance fluxes. Therefore, offline evaluation and sensitivity analysis of SLUCM can remove the uncertainty of NWP models. Of course, offline simulation cannot consider the influence of advection nor the potential interaction between adjacent grids but ensures the scheme is evaluated on its own. The parameterization of the SLUCM in WRF is coupled by using a tile approach with Noah land surface model [21]. Noah and SLUCM are run

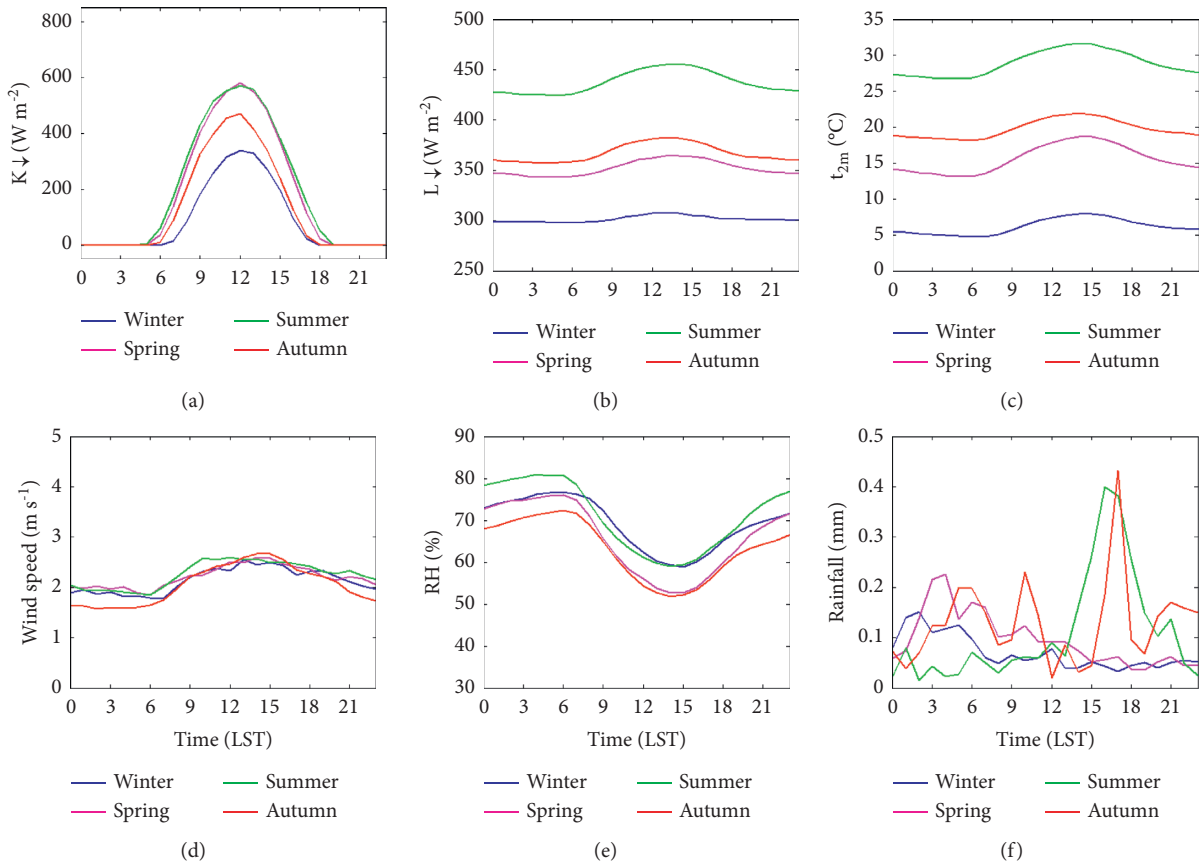

Figure 1: Seasonal mean diurnal variations of surface meteorological input variables used in the SLUCM: (a) downward shortwave radiation ($K_{\downarrow}$), (b) downward longwave radiation ($L_{\downarrow}$), (c) 2-meter air temperature (t_{2m}), (d) 10-meter wind speed, (e) 2-meter relative humidity (RH), and (f) rainfall.

independently which prevents any interaction between them, and the final output fluxes of the model are obtained according to the weighted average urban coverage ratio (f_{urb}) of the grid points, that is,

$$Q_{GRID} = Q_{SLUCM} \times f_{urb} + Q_{Noah} \times (1 - f_{urb}), \quad (5)$$

where Q_{GRID} represents the grid average modeled fluxes ($K_{\uparrow}$, $L_{\uparrow}$, Q^*, and Q_H, Q_E). f_{urb} at the XJH site is 0.86.

Based on a previous study [28], only the vegetation albedo, stomatal resistance, Zilitinkevich parameter, and LAI from the Noah LSM are ranked in the top 20 parameters with the largest influence on Q^* or Q_H. Moreover, the low vegetation and water body fraction ($f_{veg} = 0.14$) for the simulation area may also indicate small influence from Noah LSM parameters. Thus, input parameters from Noah LSM are not considered here.

SLUCM requires many input parameters, many of which are difficult to obtain in reality, so it is necessary to analyze the relative importance of each parameter. This paper uses the observational data of Shanghai XJH urban site for a whole year to drive the offline SLUCM to simulate the urban surface energy balance. The observation input fields include downward shortwave and longwave radiation flux, near surface air temperature, relative humidity, wind speed, wind direction, air pressure, and precipitation. The data for a whole year allow analyzing the seasonal variation of the surface energy balance. The flux measurements are conducted within the inertial sublayer ensuring the collected data represent local scale which matches the model scale. Since the simulated latent heat evaporation of SLUCM is limited to the precipitation period, the latent heat flux is completely calculated by the natural Noah land surface model. Previous studies have also shown that there are great systematic errors in the simulation of Q_E by SLUCM. For instance, in Marseille, France, the determination coefficients of Q_E during day and night in summer are only 0.028 and 0.006, and there is little improvement of the simulated Q_E by changing the parameters [28]. Therefore, this study focuses on the simulation capability and parameter sensitivity of SLUCM to the net all-wave radiation and sensible heat flux. It is still inspiring that efforts toward enhancing the performance of SLUCM in simulating Q_E have been made in recent years [24–26]. However, these efforts introduce additional parameters related to pervious surfaces such as trees and irrigation processes.

3. Results

3.1. Offline Evaluation of the SLUCM. Figures 3–6 show the simulated and observed average diurnal variations and scatter plots of the radiation and sensible heat flux in each

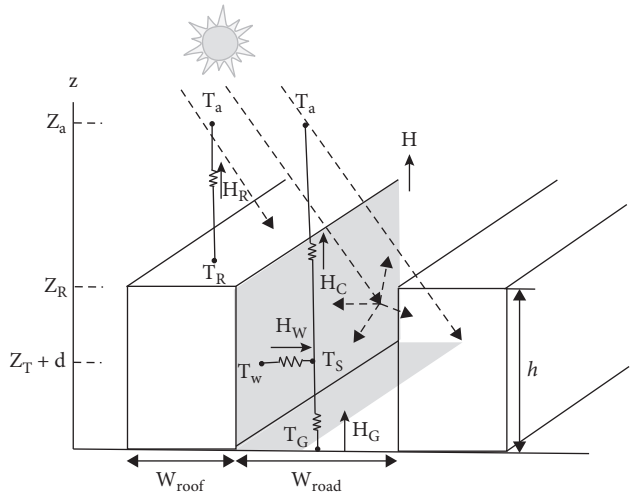

Figure 2: Diagram of the single-layer urban canopy model (SLUCM): Z_T is the roughness length for heat, Z_R (h) is the mean building height, Z_a is the bottom layer height of the parent NWP model, T_R, T_W, and T_G are roof, wall, and ground temperature, T_a is the air temperature at Z_a, T_S is the temperature defined at height $Z_T + d$, H_R represents the sensible heat flux from roof to the atmosphere, H_W and H_G are sensible heat flux from wall and ground to the urban canyon space, H is the weight-mean sensible heat flux at Z_a, and W_{roof} and W_{road} are the width of roof and road.

season using default parameter values listed in Table 1. Commonly used statistical variables (root mean square error RMSE, mean absolute error MAE, and mean deviation MBE) are used to describe the model error.

It can be seen from Figure 3 that the SLUCM successfully reproduces the diurnal pattern of the net all-wave radiation flux (Q^*) but systematically underestimates its magnitudes in all four seasons, especially the daily peak at noon with biases around 30 W m^{-2} in winter and 60 W m^{-2} in autumn, and larger deviations around 80 W m^{-2} and 90 W m^{-2} in spring and summer, respectively. SLUCM performs better at nighttime for Q^* simulation, with biases around 10 W m^{-2}. The RMSE of each season is within 19.65–42.35 W m^{-2}. The MBEs are negative except in winter (5.42 W m^{-2}).

It can be seen from Figure 4 that the SLUCM successfully reproduces the diurnal pattern of the outgoing shortwave radiation flux (K↑) in each season. The model overestimates K↑ in all four seasons, with simulated values around noon about 15 W m^{-2} greater than observations. The coefficient of determination (R^2) is larger than 0.98, the statistical RMSE is 7.31 (winter) and 9.42 W m^{-2} (Autumn), and MBE shows positive deviation in all seasons (MBE: 3.13–5.05 W m^{-2}). The simulated deviation of K↑ mainly comes from the deviation of the surface albedo.

The SLUCM also well reproduces the diurnal variation characteristics of the upward longwave radiation flux (L↑). Moreover, the occurrence time of simulated daily peaks is consistent with that of the observations (Figure 5), which appears in the afternoon. The simulated daytime L↑ has a relatively large positive bias in all seasons except in winter, while the nighttime L↑ is slightly underestimated for all seasons. The coefficients of determination (R^2) of L↑ are 0.85 (winter) and 0.96 (Autumn), RMSE is 16.29 (winter) and 35.97 W m^{-2} (summer), and MBE is 2.55 (Autumn) and 25.2 W m^{-2} (summer). The simulation error of L↑ is the main source of Q^* error.

Figure 6 shows the simulated and observed sensible heat flux (Q_H) in each season. The average observed hourly Q_H in each season is positive throughout the day; that is, the surface heats the atmosphere all day. The daily maximum of Q_H occurs in summer, followed by spring and autumn, and the minimum occurs in winter. SLUCM successfully reproduces the daily variation of Q_H, which also shows that Q_H remains positive throughout the whole day, and the daily afternoon peak is consistent with the observation. The simulated seasonal average diurnal Q_H is the lowest in winter, which is consistent with the observation, while the highest Q_H occurs in spring, which has a certain deviation from the observation. The SLUCM underestimates the average daily variation of Q_H for each season, especially in summer. The magnitudes of RMSE for Q_H in winter, spring, and autumn are similar to previous studies [28–30], which may indicate systematic errors of SLUCM. However, the magnitude of RMSE for Q_H in summer in this study is larger than that for previous studies. This may be due to the abnormally large observed Q_H caused by the extremely hot summer in 2013, which cannot be well reproduced by the SLUCM. The root mean square error (RMSE) is the smallest in winter (48.11 W m^{-2}), the largest in summer (119.13 W m^{-2}), and close in spring and autumn (70.87 and 78.63 W m^{-2}, resp.).

3.2. Parameter Sensitivity Analysis of SLUCM. In this study, the parameter sensitivity analysis of SLUCM adopts the OAT (one at a time) method [35]. The rationale is that only one parameter is changed at a time, and other parameters remain default values. In the process of changing each parameter from the minimum value to the maximum value, the step size is set to increase by 1%. Therefore, 100 times of model run is required to complete the sensitivity analysis of

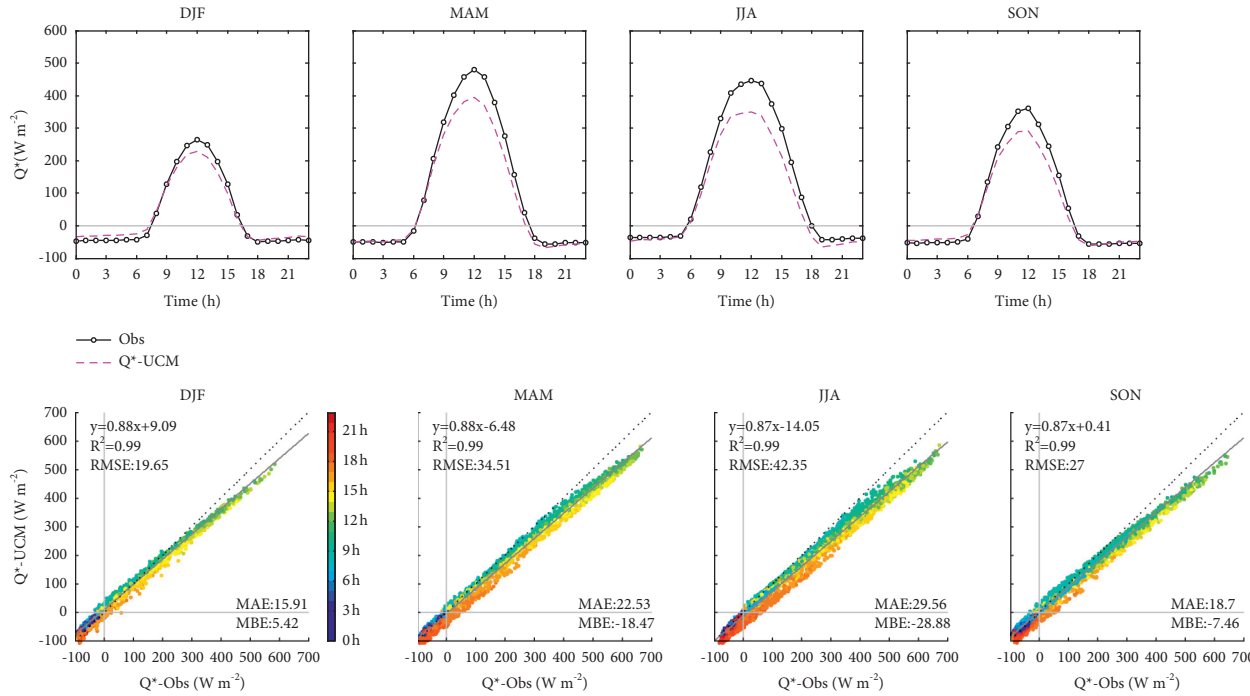

FIGURE 3: Observed (solid line) and SLUCM modeled (dotted line) seasonal mean diurnal curves of the net all-wave radiation flux (Q*, upper panel), and the lower panel is the corresponding scatter plot.

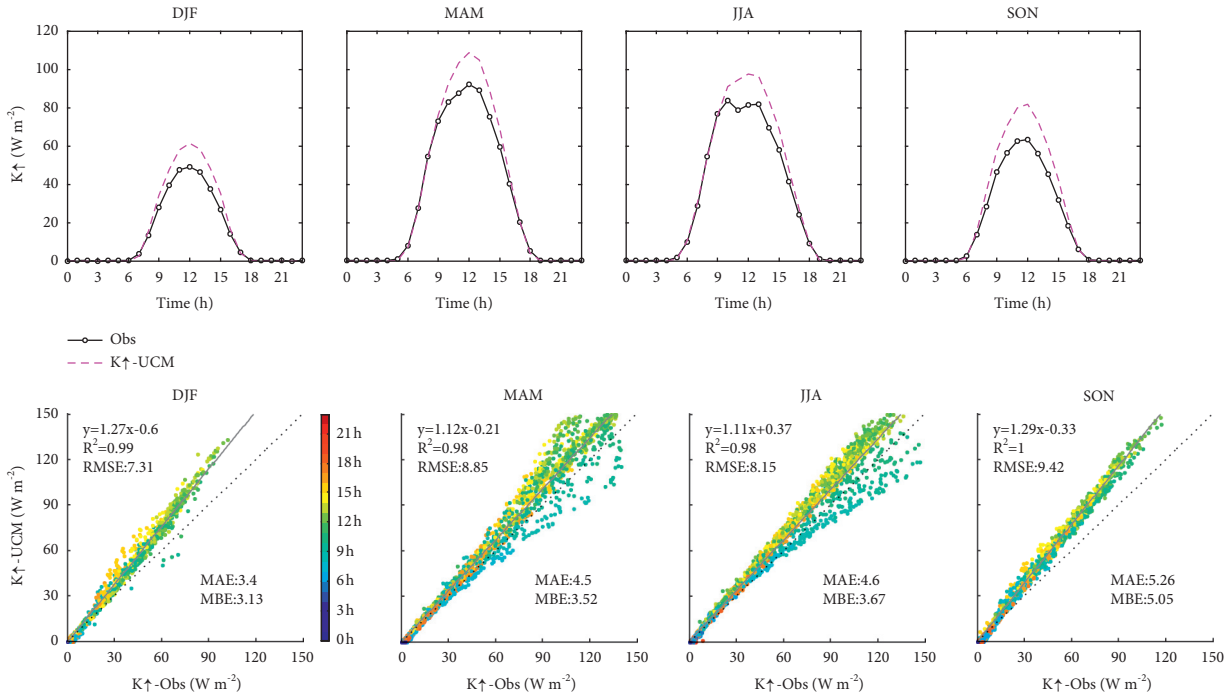

FIGURE 4: The same as Figure 3, but for the upward shortwave radiation (K↑).

each parameter. In order to improve the efficiency, here a loop is added into SLUCM to realize the automatic increment of parameters. Table 1 lists the default values and variation ranges of main parameters of SLUCM. These parameter values are mainly obtained from reference [28]. For such a list of parameter sets, it mainly includes the definition of urban geometry, radiation attributes, heat capacity, thermal conductivity, and so on.

In order to study the sensitivity of surface fluxes to model parameters and the characteristics of variations with parameters, Figures 7–11 show variations of mean surface fluxes and RMSE with parameters. Figure 7 shows variation

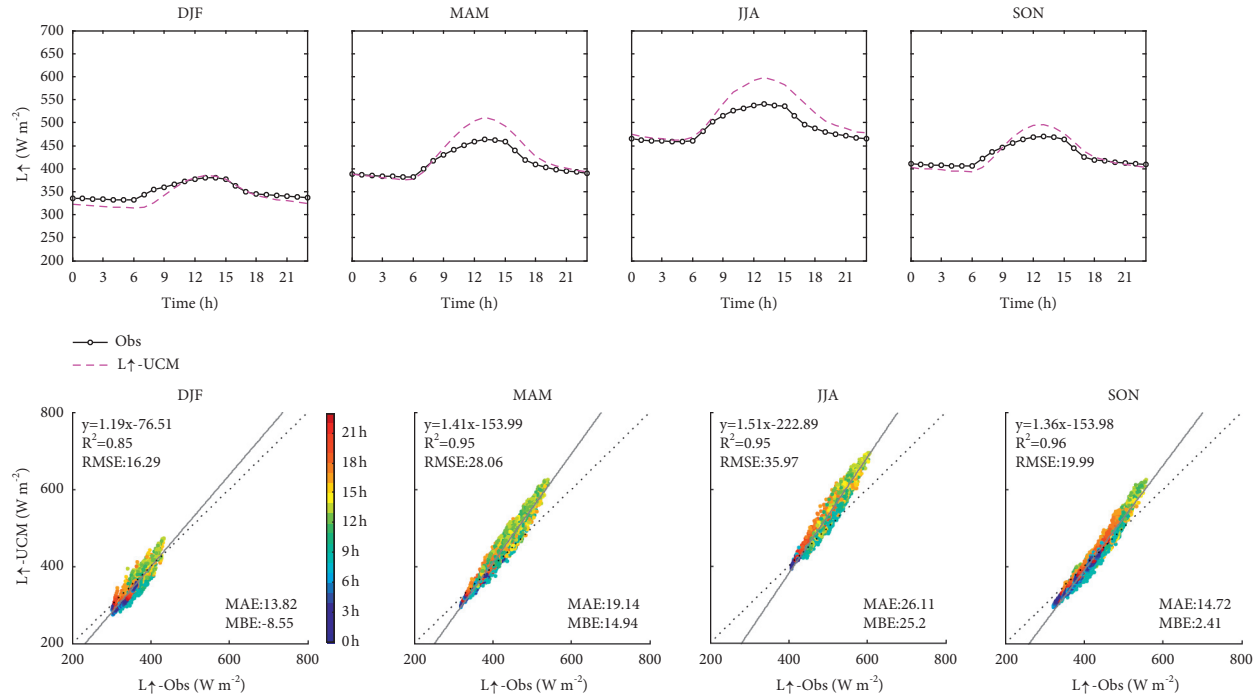

FIGURE 5: The same as Figure 3, but for the upward longwave radiation (L↑).

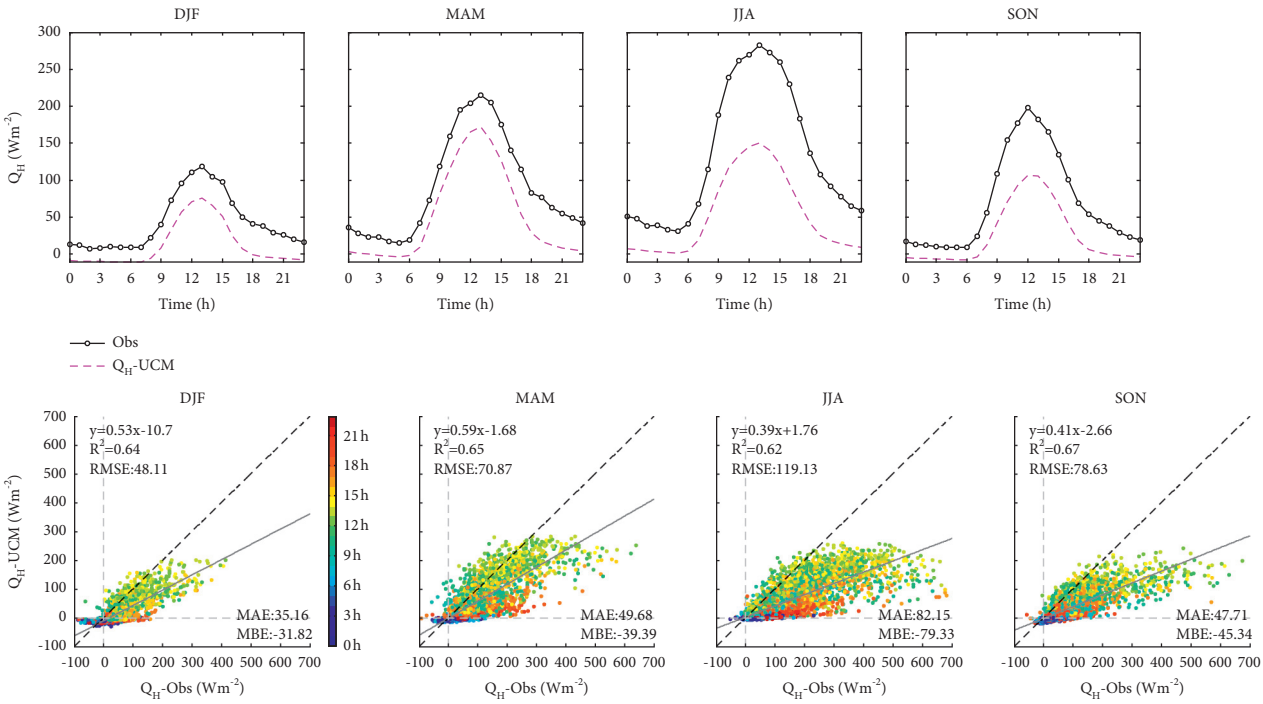

FIGURE 6: The same as Figure 3, but for the sensible heat flux (Q_H).

characteristics of each flux with roof, wall, and ground albedo (ALBR/ALBB/ALBG). The influence of the surface albedo of the three facets on the net all-wave radiation flux (Q^*) is mainly linearly distributed. During the day, Q^* is very sensitive to the albedo of the roof and wall. With the increase of albedo, Q^* decreases rapidly. When ALBR or ALBB increase by 0.01, Q^* decreases by about 1.4 and 0.9 W m^{-2}, respectively. The impact of surface albedo on Q^* includes both direct and indirect aspects: the direct impact is that a large albedo causes a large upward reflected shortwave radiation (K↑), which reduces the net shortwave radiation flux to the surface, thus reduces the simulated surface temperature, and finally causes an indirect impact of reducing the upward longwave radiation (L↑). It can be seen

Table 1: SLUCM input parameters selected for analysis, value space, and default values.

Parameter	Min.	Max.	Default	Definition (unit)
ALBR	0.05	0.4	0.2	Roof albedo (-)
ALBB	0.05	0.55	0.2	Wall albedo (-)
ALBG	0.05	0.3	0.2	Road albedo (-)
EPSR	0.85	0.98	0.9	Roof emissivity (-)
EPSB	0.85	0.98	0.9	Wall emissivity (-)
EPSG	0.85	0.98	0.9	Road emissivity (-)
AKSR	0.04	1.74	0.67	Roof conductivity (W/m/K)
AKSB	0.04	1.74	0.67	Wall conductivity (W/m/K)
AKSG	0.04	1.74	0.67	Road conductivity (W/m/K)
CAPR	0.1 E6	2.3 E6	1 E6	Roof capacity (J $m^{-3}K^{-1}$)
CAPB	0.1 E6	2.2 E6	1 E6	Wall capacity (J $m^{-3}K^{-1}$)
CAPG	0.3 E6	2.1 E6	1.4 E6	Road capacity (J $m^{-3}K^{-1}$)
Z_R	10	60	20	Roof height (m)
W_{roof}	10	40	20	Roof width (m)
W_{road}	10	40	20	Road width (m)

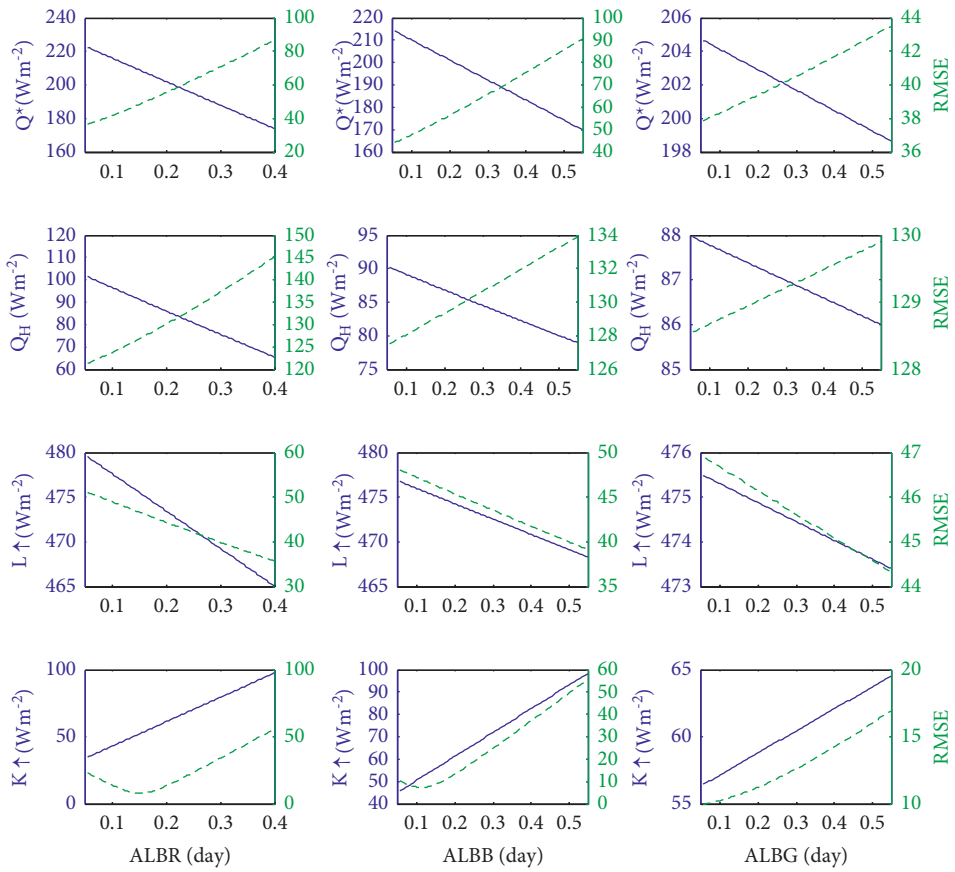

Figure 7: Variations of the mean (blue solid line) and RMSE (green dashed line) of the net all-wave radiation (Q^*), sensible heat flux (Q_H), upward longwave radiation (L↑), and shortwave radiation (K↑) with roof (ALBR), wall (ALBB), and road (ALBG) albedo parameters during daytime.

that both K↑ and L↑ change linearly with the albedo. However, the effect of surface albedo on K↑ and L↑ is opposite. Meanwhile, the influence of surface albedo on K↑ is significantly greater than that of L↑, resulting in a negative effect on Q^*. Compared with the roof and wall albedo, Q^* is relatively insensitive to the ground albedo. For every 0.01 increase in ground albedo (ALBG), Q^* decreases by about 0.2 W m^{-2}. In addition, it can be seen that when ALBR = 0.15 and ALBB = 0.11, the RMSE of K↑ reaches the minimum, which is consistent with the observed albedo values.

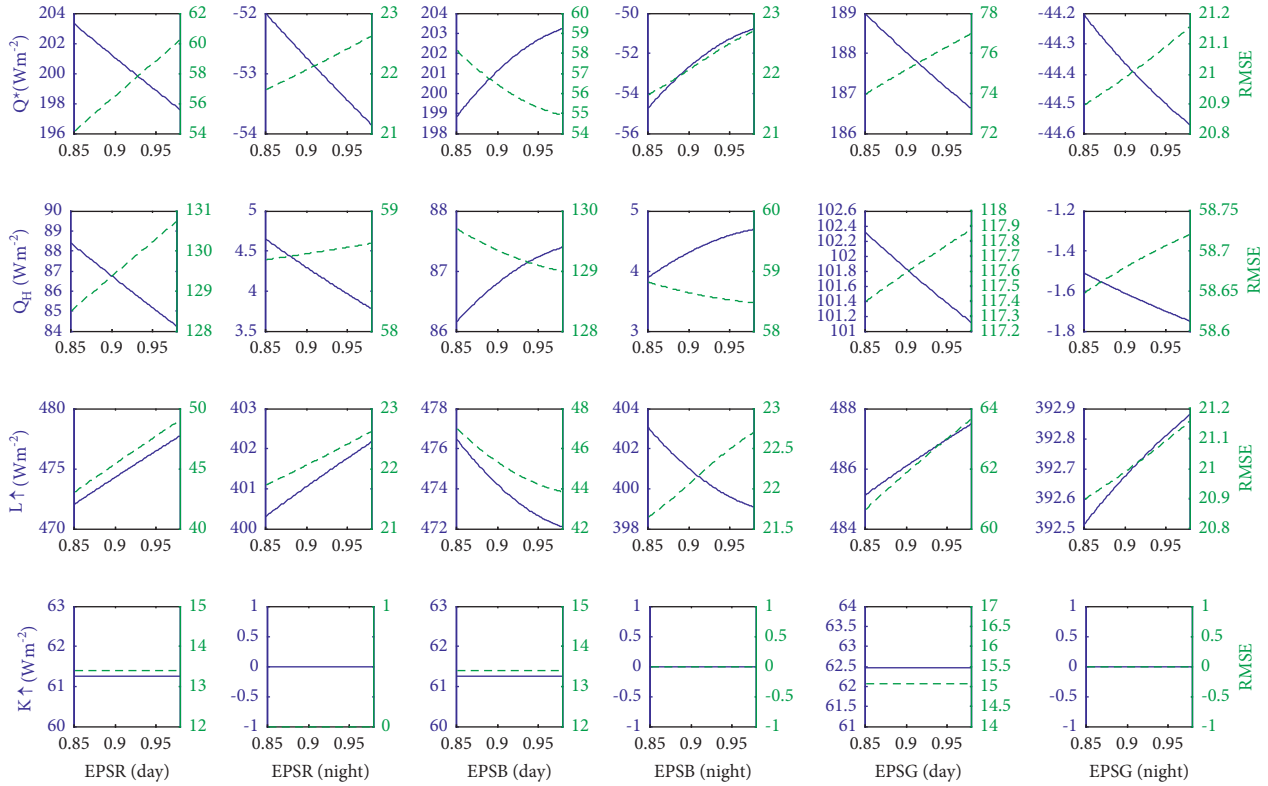

Figure 8: The same as Figure 7, but for roof (EPSR), wall (EPSB), and road (EPSG) emissivity parameters.

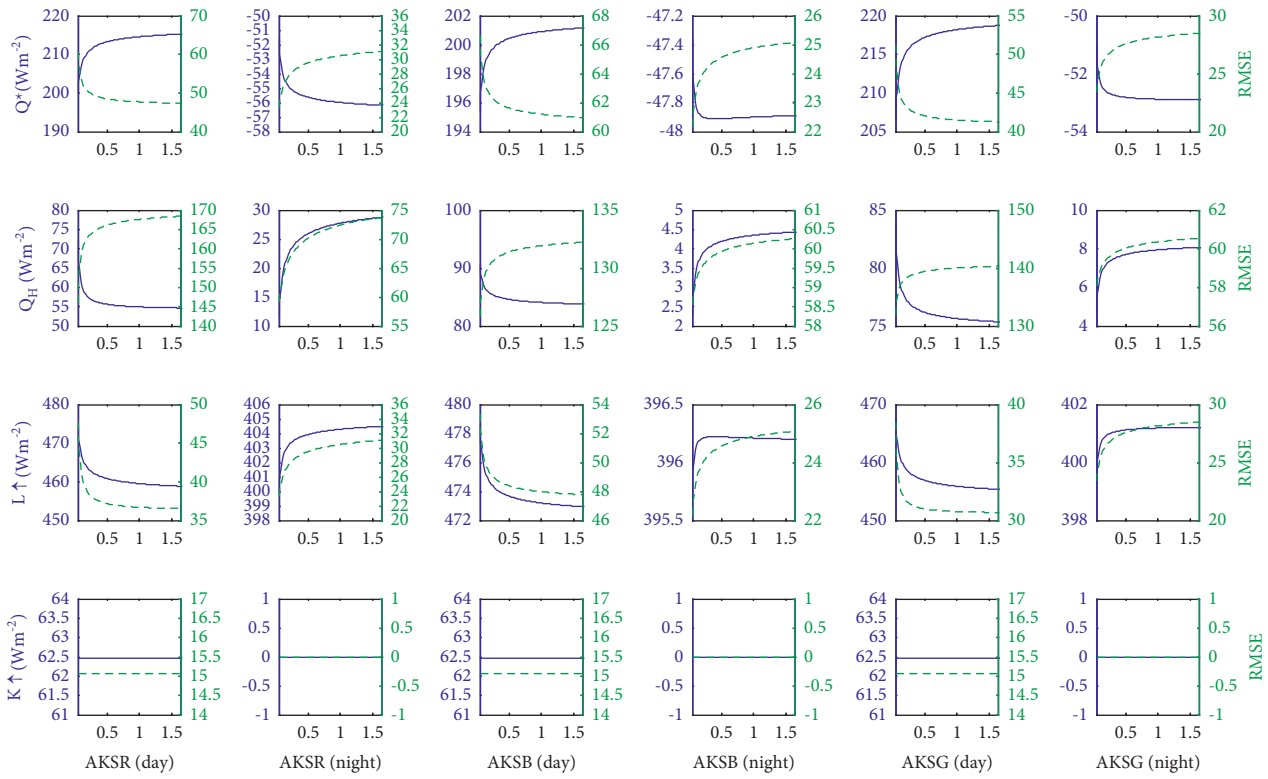

Figure 9: The same as Figure 7, but for conductivity parameters.

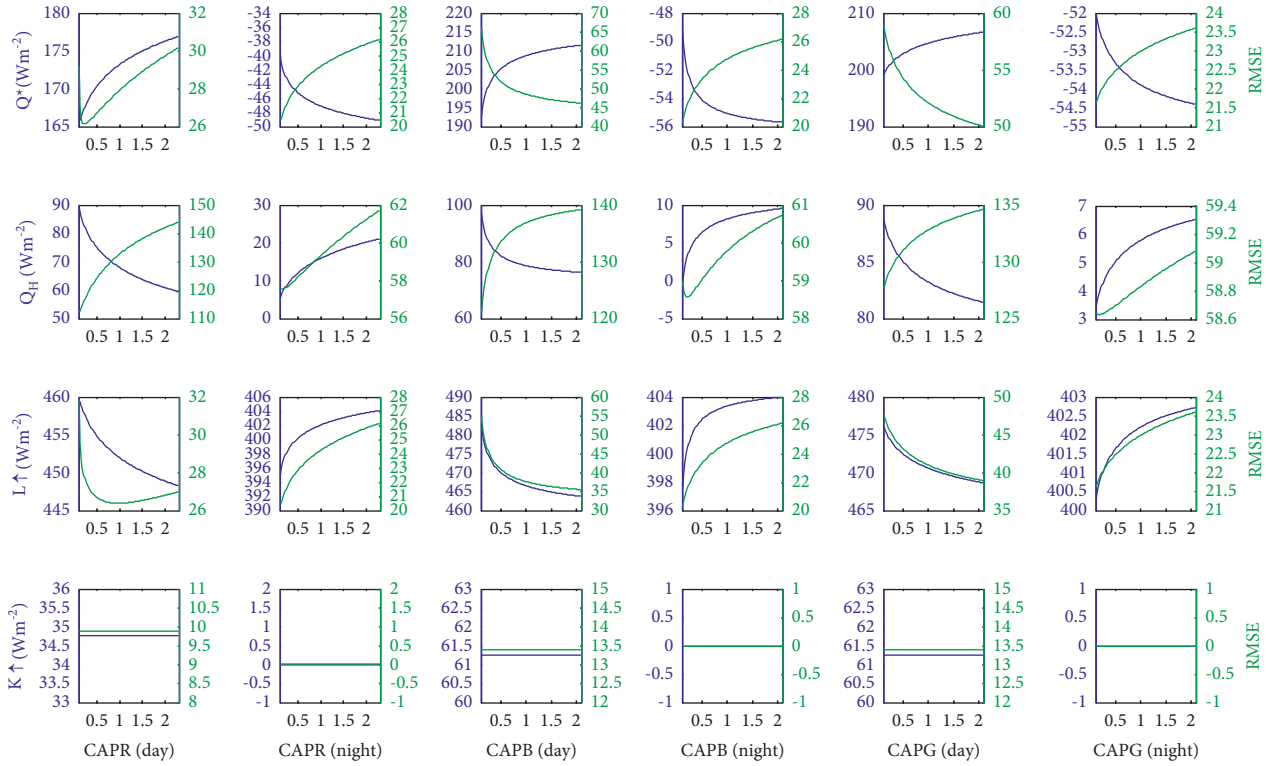

Figure 10: The same as Figure 7, but for capacity parameters.

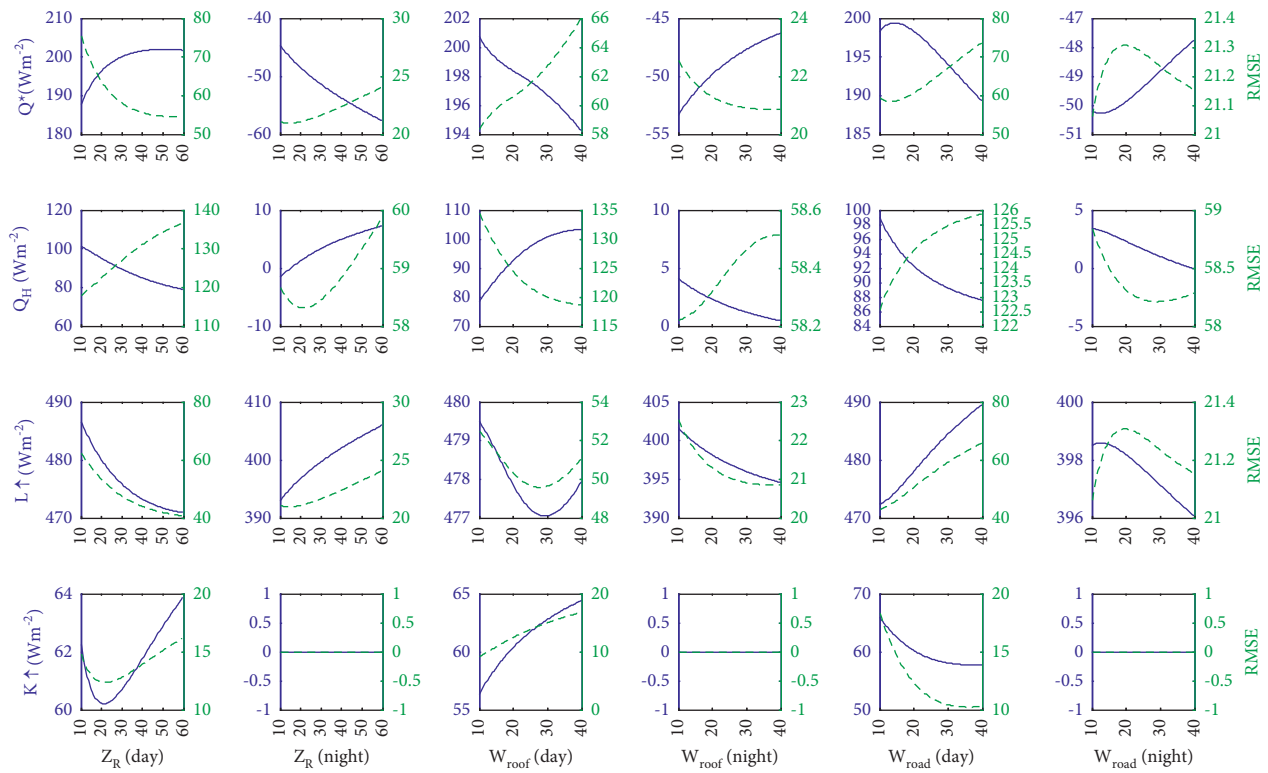

Figure 11: The same as Figure 7, but for morphological parameters.

Based on previous studies conducted in different cities such as Marseille, France [28], Princeton, USA [29], and Nanjing, China [30], variability in roof (followed by wall) parameters has always been shown to be the most important factor for the SLUCM. Our results are consistent with these studies. This may be due to the direct impact from roof surfaces on the simulated fluxes and the obstruction of roofs on roads at this high-rise and densely built-up site. This conclusion has been applied to many urban heat island mitigation strategies by designing green or white roofs with larger evaporative potential or surface albedo [36–39].

The sensitivity of the surface emissivity to each flux is not as strong as that of the surface albedo, and the variation trend is also linear. The daytime Q^* decreases with the increase of emissivity, which is attributed to the increase of L↑ caused by the increase of emissivity. Similar to surface albedo, each flux is most sensitive to roof emissivity (EPSR), followed by wall emissivity (EPSR), and the least sensitive to road emissivity (EPSR). When EPSR, EPSB, and EPSG increase by 0.01, Q^* decreases by 1, 0.2, and 0.1 W m^{-2}, respectively. When EPSR and EPSG values are relatively small, RMSE for each flux is also small no matter during the day or night. When EPSB is relatively large, RMSE for Q^* is relatively small during the day while being relatively large at night, and RMSE for Q_H stays small during the day and night. The variation of Q_H with albedo and emissivity is also linear, and the variation characteristics are largely consistent with Q^*.

The influence of thermal parameters (surface heat capacity and conductivity) on fluxes is logarithmic, which indicates that, with the increase of parameter values, the sensitivity of fluxes to thermal parameters decreases rapidly. When the thermal conductivity for the three urban facets (AKSR, AKSB, and AKSG) is greater than 0.5 W $m^{-1}k^{-1}$, the variation range of surface fluxes becomes very small, while below this value, the variation is much more intense. Similarly, surface fluxes are more sensitive to thermal parameters of roof and wall, but less sensitive to thermal parameters of the road. Thermal parameters mainly impact sensible heat flux and longwave radiation flux through changing surface temperature.

The variation characteristics of RMSE for Q^* with the thermal conductivity (AKS) during the daytime are that the RMSE decreases rapidly with AKS when the AKS is small and then tends to be relatively stable. The variation pattern at night is opposite to that during the day. The variation of RMSE for Q_H with AKS is opposite to Q^* during the day, while the variation trend of RMSE at night is consistent with Q^*. Therefore, when considering the optimization of several parameters at the same time, it is impossible to achieve the minimum RMSE satisfying Q^* and Q_H simultaneously. This is determined by the nature of uncertainty theory. The variation characteristics of RMSE with CAP is similar to that of AKS. Both Q^* and Q_H show the strongest sensitivity to roof parameters, mainly due to the rooftop position of measurement instruments and the obstruction of roofs on roads at this high-rise and densely built-up site which results in the dominant impact of roofs. Wall parameters are second sensitive for Q^* and Q_H, while road parameters are not sensitive for Q^* and Q_H. Therefore, roof and wall parameters need to be taken into account more carefully than road parameters.

For morphometric parameters (Figure 11), K↑ increases with the increase of W_{roof}, which may be attributed to the relative decrease of urban canyon width that reduces the trapping effect of the urban canyon on radiation, thus increasing K↑. Both W_{roof} and W_{road} are involved in the parameterization of urban canyon and roof roughness, which make their impact on Q_H complicated. The sensitivity curves of surface fluxes to geometric parameters have no specific variation patterns. For daytime Q^*, it increases rapidly with building height (Z_R) and changes gently with Z_R when $Z_R > 25$ m. This may be because when Z_R is less than 20 m, the radiation effect of urban canyon on upward shortwave and longwave radiation is negative in both cases, with larger effect on upward longwave radiation. The superposition of the two effects makes Q^* increase more rapidly. When $Z_R > 20$ m, the radiation effect on upward shortwave and longwave radiation is opposite, which offset with each other, making Q^* change slowly. At night, Q^* decreases linearly with Z_R, which may be due to the increase of daytime storage in the urban canopy with the increase of buildings, so that more longwave radiation flux can be released at night.

The variation of Q^* with Z_R increases gradually during daytime (Figure 11). This is because L↑ decreases more sharply than the increase of K↑ during daytime. The change of Q_H with Z_R is linear which decreases linearly during the day (the decrease range is about 20 W m^{-2}) and increases linearly at night (the increase range is about 9 W m^{-2}).

Q^* decreases with the increase of roof width (W_{roof}) during the daytime. This is because, with the increase of W_{roof}, K↑ increases almost linearly, while L↑ decreases firstly and then increases with the increase of W_{roof}, and the decreasing range is less than the increase of K↑. This results in the constant decrease of Q^*, but with slightly smaller decreasing range at the beginning than that in the later stage. For longwave radiation, on the one hand, wider roofs (thus relatively narrower urban canyons as all types of urban canyon facets are normalized by $W_{roof} + W_{road}$) make more longwave radiation trapped within the canyon; on the other hand, wider roofs also release more upward longwave radiation. The sensible heat flux (Q_H) increases with W_{roof}, which may be caused by interception, and then the increase trend slows down, which may be because the interception is no longer dominant. The nighttime Q^* increases with W_{roof}. This is due to the reduction of Q^* absorbed during the day that reduces the heat storage at night, resulting in the reduction of longwave radiation released at night. Q^* increases firstly with W_{road} and reaches the maximum with RMSE reaching the minimum around 15 m and then decreases with W_{road} during daytime. The sensitivity of Q^* to W_{road} at night is smaller than that at daytime with opposite pattern. Both L↑ and RMSE of L↑ increase with W_{road} during daytime. The pattern for K↑ with W_{road} is opposite to L↑ with smaller sensitivity during daytime. The variation of Q_H with W_{road} is similar to Q^* during daytime and not sensitive at night.

Table 2: The default and optimized SLUCM parameters.

Parameter	Optimum	Default	Definition (unit)
ALBR	0.16	0.2	Roof albedo (-)
ALBB	0.14	0.2	Wall albedo (-)
ALBG	0.13	0.2	Road albedo (-)
EPSR	0.85	0.9	Roof emissivity (-)
EPSB	0.95	0.9	Wall emissivity (-)
EPSG	0.95	0.9	Road emissivity (-)
AKSR	0.6	0.67	Roof conductivity (W $m^{-1} K^{-1}$)
AKSB	0.67	0.67	Wall conductivity (W $m^{-1} K^{-1}$)
AKSG	0.4	0.67	Road conductivity (W $m^{-1} K^{-1}$)
CAPR	1.4E6	1.0 E6	Roof capacity (J $m^{-3} K^{-1}$)
CAPB	1.0E6	1.0 E6	Wall capacity (J $m^{-3} K^{-1}$)
CAPG	1.4E6	1.4 E6	Road capacity (J $m^{-3} K^{-1}$)
Z_R	36	20	Roof height (m)
W_{roof}	25	20	Roof width (m)
W_{road}	15	20	Road width (m)

Table 3: Comparison of RMSE for each flux before and after parameter optimization.

Season	RMSE (W m^{-2})	Q^*	K↑	L↑	Q_H
Winter	RMSE before	19.65	7.31	16.29	48.11
	RMSE after	16.23	3.69	15.05	45.97
Spring	RMSE before	34.51	8.85	28.06	70.87
	RMSE after	20.99	5.58	20.46	67.32
Summer	RMSE before	42.35	8.15	35.97	119.13
	RMSE after	28.8	5.18	28.1	113.92
Autumn	RMSE before	27.0	9.42	19.99	78.63
	RMSE after	18.66	4.54	15.98	75.46

3.3. Parameter Optimization of SLUCM. OAT parameter sensitivity analysis method has the advantages of simplicity, direct data analysis, and easy interpretation. However, the default parameter values need to be set in advance which has potential impacts on the sensitivity analysis results, and the interaction between various parameters is not considered.

Firstly, the radiation fluxes as the input energy source of urban surface-atmosphere exchanges and with relatively small observation error are optimized according to the observation of upward and downward longwave and shortwave radiation flux at the XJH flux site and the curve characteristics of the above parameter sensitivity tests. Parameters affecting the shortwave radiation flux mainly include surface albedo and morphological parameters, which can be calculated according to the actual geographic information data without estimation. Since SLUCM overestimates the upward shortwave radiation flux (K↑) in the four seasons, it is necessary to reduce the default surface albedo of the three facets. Using the permutation and combination method, the albedo of the three facets is firstly optimized so as to reduce the simulated RMSE of K↑ as much as possible. On this basis, the surface emissivity is optimized with reference to the sensitive curve characteristics of net all-wave radiation flux and sensible heat flux, and the optimal values of other thermal parameters are determined lastly. The final optimized parameter values are listed in Table 2.

The simulation statistics (RMSE) for each flux using the optimized parameter set are given in Table 3 and Figure 12. It can be seen that SLUCM has significantly improved the simulation of net radiation flux (Q^*), upward shortwave radiation flux (K↑), upward longwave radiation flux (L↑), and sensible heat flux (Q_H) after parameter adjustment. The improvement of K↑ in autumn and winter was more obvious than that in spring and summer with RMSE decreased from 9.42 to 7.31 W m^{-2} to 4.54 and 3.69 W m^{-2}, while RMSE decreased by about 3 W m^{-2} in spring and summer. SLUCM still slightly overestimates K↑ in autumn and winter (MBE >0), while the simulation of K↑ in spring and summer shifted to a slightly underestimated trend (MBE <0). This is mainly due to the seasonal variation of albedo, which is not considered here by SLUCM. The RMSE of Q^* in the four seasons decreases by about 3.4–18.7 W m^{-2}. The RMSE for L↑ decreases significantly in spring and summer by about 8 W m^{-2}, but only about 1.2 W m^{-2} in winter. SLUCM slightly improves Q_H with RMSE reduced by about 2–5 W m^{-2}. The latent heat flux (Q_E) is poorly simulated and the optimized parameters have little impact on Q_E. Thus, improving the urban hydrological processes in SLUCM is of great importance in the future.

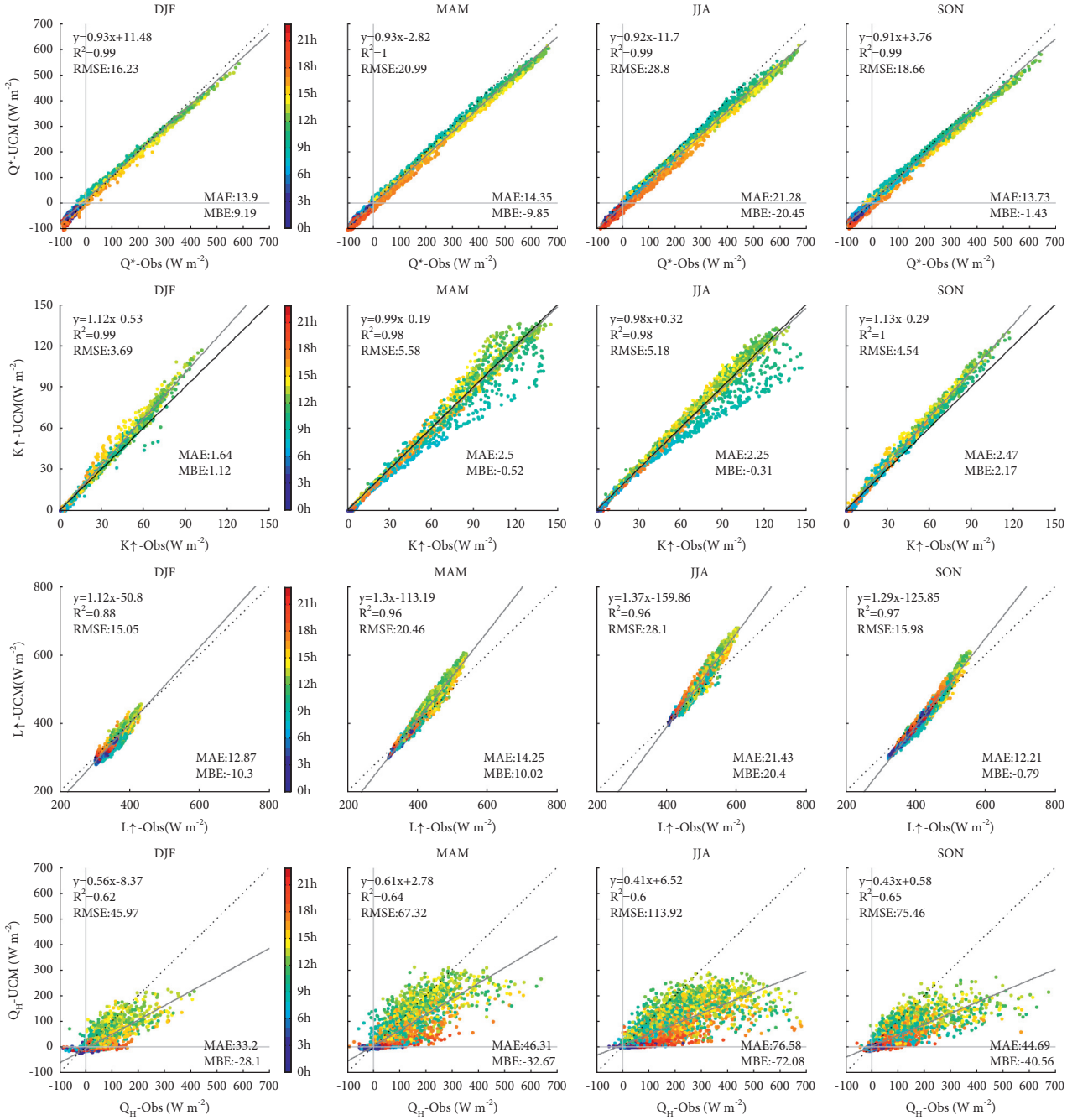

FIGURE 12: Scatter plots of observed and modeled fluxes after parameter optimization. The dot colors represent the hours, R^2, RMSE, MAE, and MBE are given.

4. Conclusions and Discussions

In this paper, the offline SLUCM model is evaluated by a full-year observation data from Shanghai central urban flux site. The simulation capability of SLUCM for net all-wave radiation flux and sensible heat flux is particularly analyzed, and the sensitivity of a series of parameters is tested by the OAT method. Finally, according to the observed flux data and referring to the characteristics of sensitivity curves of various parameters, optimized parameter values of SLUCM suitable for Shanghai urban area are given. The main conclusions are as follows:

(1) The offline simulation results show that the SLUCM model can successfully reproduce the daily variation of the net all-wave radiation flux (Q^*) but systematically slightly underestimate the magnitude of Q^* in four seasons. The error of Q^* is mainly caused by the relatively poor simulation ability for the upward longwave radiation. SLUCM successfully simulates

the diurnal pattern of the sensible heat flux (Q_H), which remains positive throughout the whole day. The simulated occurrence time of the diurnal peaks for Q_H is consistent with observations. The average daily variations of Q_H are underestimated in each season especially in summer, which may be due to the abnormally large observed sensible heat flux caused by the extremely high temperature in summer 2013 that the SLUCM fails to well reproduce this extreme value.

(2) The parameter sensitivity analysis shows that Q^* changes with the surface albedo linearly and is the most sensitive to the roof albedo, followed by the wall albedo. With the increase of surface albedo, Q^* decreases rapidly. Q^* is relatively insensitive to the ground albedo. Q^* is less sensitive to surface emissivity compared to surface albedo, but the variation trend is also linear. Similar to surface albedo, each flux is most sensitive to roof emissivity. This might be due to the rooftop position of in situ measurements and the obstruction of roofs on roads with high-rise buildings around the site. The variation of sensible heat flux (Q_H) with albedo and emissivity is also linear, and the variation characteristics are basically consistent with Q^*. The influence of thermal parameters on flux is logarithmic; that is, with the increase of parameters, the sensitivity of flux to thermal parameters decreases. Similarly, surface fluxes are more sensitive to the thermal parameters of roof and wall, but less sensitive to the thermal parameters of road. The sensitivity curves of surface fluxes to geometric parameters have no specific variation patterns.

(3) After parameter optimization, the simulation errors (RMSE) of upward shortwave radiation flux (K↑), upward longwave radiation flux (L↑), net radiation flux (Q^*), and sensible heat flux (Q_H) all decrease. The improvement of the simulated K↑ in autumn and winter is more obvious than that in spring and summer, while the improvement of the simulated L↑ in spring and summer is more obvious than that in autumn and winter. SLUCM still slightly overestimates K↑ in autumn and winter, while the simulation of K↑ in spring and summer is slightly underestimated. This is mainly due to the seasonal variation of the surface albedo which is not considered by SLUCM. The RMSE of Q^* in the four seasons decreases by about 3.4–18.7 W m^{-2}. The RMSE of L↑ decreases by about 1.2–7.87 W m^{-2}. The RMSE of sensible heat flux (Q_H) decreases by about 2–5 W m^{-2}.

This study shows that there are obvious seasonal differences in the improvement of each flux using the optimized parameter values of SLUCM; thus, parameters need to be optimized by season in future studies. The OAT method used for parameter sensitivity analysis does not consider the interaction among parameters. In the next step, other multiobjective parameter optimization schemes can be considered [28, 29]. In addition, this study only tests and optimizes the sensitivity of SLUCM parameters in the offline mode. When SLUCM is coupled to the mesoscale WRF numerical weather prediction model for online simulation, the meteorological forcing variables of SLUCM are provided by the parent WRF model, and the influence of advection is also considered in the online simulation. There are many differences in the response to parameters between online and offline simulation. It is still very necessary to further carry out online simulation and evaluation in the future.

Data Availability

The raw data are not freely available, but postprocessed data can be shared.

Conflicts of Interest

The authors declare no conflicts of interest.

Acknowledgments

This study was funded by the National Natural Science Foundation of China (Grant nos. 42005077 and U2142206), Shanghai Sailing Program (Grant no. 19YF1443900), the National Key Research and Development Program of China (no. 2021YFC3000800), and the National Natural Science Foundation of China (Grant nos. 42105152, 42005144, 42075012, and 41875059). The authors thank those who contributed to data processing and model evaluation.

References

[1] J. P. Quan, Y. K. Xue, and Q. Y. Duan, "Numerical investigation and uncertainty analysis of East China's large-scale urbanization effect on regional climate," *Journal of Meteorological Research*, vol. 35, no. 6, pp. 1–18, 2021.

[2] G. Ren, Y. Ding, and G. Tang, "An overview of mainland China temperature change research," *Journal of Meteorological Research*, vol. 31, no. 1, pp. 3–16, 2017.

[3] X. Yang, L. Ruby Leung, N. Zhao et al., "Contribution of urbanization to the increase of extreme heat events in an urban agglomeration in east China," *Geophysical Research Letters*, vol. 44, no. 13, pp. 6940–6950, 2017.

[4] N. Zhang and Y. Chen, "A case study of the upwind urbanization influence on the urban heat island effects along the suzhou-wuxi corridor," *Journal of Applied Meteorology and Climatology*, vol. 53, no. 2, pp. 333–345, 2014.

[5] C. Zhao, Q. Jiang, Z. Sun, H. Zhong, and S. Lu, "Projected urbanization impacts on surface climate and energy budgets in the Pearl River Delta of China," *Advances in Meteorology*, vol. 2013, Article ID 542086, 10 pages, 2013.

[6] D. Li, T. Sun, M. Liu, L. Yang, L. Wang, and Z. Gao, "Contrasting responses of urban and rural surface energy budgets to heat waves explain synergies between urban heat islands and heat waves," *Environmental Research Letters*, vol. 10, no. 5, p. 054009, 2015.

[7] L. Zhao, M. Oppenheimer, Q. Zhu et al., "Interactions between urban heat islands and heat waves," *Environmental Research Letters*, vol. 13, no. 3, p. 034003, 2018.

[8] X. Ao, L. Wang, X. Zhi, W. Gu, H. Yang, and D. Li, "Observed synergies between urban heat islands and heat waves and their controlling factors in Shanghai, China," *Journal of Applied Meteorology and Climatology*, vol. 58, no. 9, pp. 1955–1972, 2019.

[9] C. S. B. Grimmond, M. Blackett, M. J. Best et al., "The international urban energy balance models comparison project: first results from phase 1," *Journal of Applied Meteorology and Climatology*, vol. 49, no. 6, pp. 1268–1292, 2010.

[10] Z. Xie, B. Liu, X. Yan et al., "Effects of implementation of urban planning in response to climate change," *Progress in Geography*, vol. 39, no. 1, pp. 120–131, 2020.

[11] K. W. Oleson, G. B. Bonan, J. Feddema, and M. Vertenstein, "An urban parameterization for a global climate model. Part II: sensitivity to input parameters and the simulated urban heat island in offline simulationsfline simulations," *Journal of Applied Meteorology and Climatology*, vol. 47, no. 4, pp. 1061–1076, 2008.

[12] A. Baklanov, J. Ching, C. S. B. Grimmond, and A. Martilli, "Model urbanization strategy: summaries, recommendations and requirements," *Meteorological and Air Quality Models for Urban Areas*, Springer, Berlin, Heidelberg, 2009.

[13] S. R. Shaffer, W. T. L. Chow, M. Georgescu et al., "Multiscale modeling and evaluation of urban surface energy balance in the phoenix metropolitan area," *Journal of Applied Meteorology and Climatology*, vol. 54, no. 2, pp. 322–338, 2015.

[14] S. Miao, W. Jiang, P. Liang et al., "Advances in urban meteorological research in China," *Journal of Meteorological Research*, vol. 34, no. 2, pp. 218–242, 2020.

[15] L. Jarvi, C. S. B. Grimmond, and A. Christen, "The surface urban energy and water balance scheme (SUEWS): evaluation in Los Angeles and Vancouver," *Journal of Hydrology*, vol. 411, no. 3, pp. 219–237, 2011.

[16] X. Ao, C. S. B. Grimmond, H. C. Ward et al., "Evaluation of the surface urban energy and water balance scheme (SUEWS) at a dense urban site in Shanghai: sensitivity to anthropogenic heat and irrigation," *Journal of Hydrometeorology*, vol. 19, no. 12, pp. 1983–2005, 2018.

[17] H. Kusaka, H. Kondo, Y. Kikegawa, and F. Kimura, "A simple single-layer urban canopy model for atmospheric models: comparison with multi-layer and slab models," *Boundary-Layer Meteorology*, vol. 101, no. 3, pp. 329–358, 2001.

[18] V. Masson, "A physically-based scheme for the urban energy budget in atmospheric models," *Boundary-Layer Meteorology*, vol. 94, no. 3, pp. 357–397, 2000.

[19] A. Martilli, A. Clappier, and M. W. Rotach, "An urban surface exchange parameterisation for mesoscale models," *Boundary-Layer Meteorology*, vol. 104, no. 2, pp. 261–304, 2002.

[20] W. C. Skamarock, J. B. Klemp, and J. Dudhia, "A description of the advanced research WRF version 3," *NCAR Tech Note TN-475+STR*, vol. 125, 2005.

[21] F. Chen, X. Yang, and W. Zhu, "WRF simulations of urban heat island under hot-weather synoptic conditions: the case study of Hangzhou City, China," *Atmospheric Research*, vol. 138, pp. 364–377, 2014.

[22] M. Yu, S. Miao, and Q. Li, "Synoptic analysis and urban signatures of a heavy rainfall on 7 August 2015 in Beijing," *Journal of Geophysical Research: Atmospheres*, vol. 122, no. 1, pp. 65–78, 2017.

[23] N. Zhang, Y. Chen, and H. Gao, "Influence of urban land cover data uncertainties on the numerical simulations of urbanization effects in the 2013 high-temperature episode in Eastern China," *Theoretical and Applied Climatology*, vol. 138, no. 3, pp. 1715–1734, 2019.

[24] S. Miao and F. Chen, "Enhanced modeling of latent heat flux from urban surfaces in the Noah/single-layer urban canopy coupled model," *Science China Earth Sciences*, vol. 57, no. 10, pp. 2408–2416, 2014.

[25] J. Yang, Z.-H. Wang, F. Chen et al., "Enhancing hydrologic modelling in the coupled weather research and forecasting-urban modelling system," *Boundary-Layer Meteorology*, vol. 155, no. 1, pp. 87–109, 2015.

[26] C. Wang, Z.-H. Wang, and Y.-H. Ryu, "A single-layer urban canopy model with transmissive radiation exchange between trees and street canyons," *Building and Environment*, vol. 191, p. 107593, 2021.

[27] M. Demuzere, S. Harshan, L. Järvi et al., "Impact of urban canopy models and external parameters on the modelled urban energy balance in a tropical city," *Quarterly Journal of the Royal Meteorological Society*, vol. 143, no. 704, pp. 1581–1596, 2017.

[28] T. Loridan, C. S. B. Grimmond, and S. Grossman-Clarke, "Trade-offs and responsiveness of the single-layer urban canopy parametrization in WRF: an offline evaluation using the MOSCEM optimization algorithm and field observations," *Quarterly Journal of the Royal Meteorological Society*, vol. 136, pp. 997–1019, 2011.

[29] Z. Wang, B. Elie, and A. Kui, "Analyzing the sensitivity of WRF's single-layer urban canopy model to parameter uncertainty using advanced Monte Carlo simulation," *Journal of Applied Meteorology and Climatology*, vol. 50, no. 9, pp. 1795–1814, 2015.

[30] W. Zhao, N. Zhang, J. Sun, and J. Zou, "Evaluation and parameter-sensitivity study of a single-layer urban canopy model (SLUCM) with measurements in Nanjing, China," *Journal of Hydrometeorology*, vol. 15, no. 3, pp. 1078–1090, 2014.

[31] X. Zhang, Y. Yang, and B. Chen, "Operational precipitation forecast over China using the weather research and forecasting (WRF) model at a gray-zone resolution: impact of convection parameterization," *Weather and Forecasting*, vol. 36, no. 3, pp. 915–928, 2021.

[32] X. Ao, C. S. B. Grimmond, Y. Chang et al., "Heat, water and carbon exchanges in the tall megacity of Shanghai: challenges and results," *International Journal of Climatology*, vol. 36, no. 14, pp. 4608–4624, 2016.

[33] F. Chen, H. Kusaka, R. Bornstein et al., "The integrated WRF/urban modelling system: development, evaluation, and applications to urban environmental problems," *International Journal of Climatology*, vol. 31, no. 2, pp. 273–288, 2011.

[34] R. W. MacDonald, R. F. Griffiths, and D. J. Hall, "An improved method for the estimation of surface roughness of obstacle arrays," *Atmospheric Environment*, vol. 32, no. 11, pp. 1857–1864, 1998.

[35] A. J. Pitman, "Assessing the sensitivity of a land-surface scheme to the parameter values using a single column model," *Journal of Climate*, vol. 7, no. 12, pp. 1856–1869, 1994.

[36] D. Li, E. Bou-Zeid, and M. Oppenheimer, "The effectiveness of cool and green roofs as urban heat island mitigation strategies," *Environmental Research Letters*, vol. 9, no. 5, p. 055002, 2014.

[37] T. Sun, C. S. B. Grimmond, and G.-H. Ni, "How do green roofs mitigate urban thermal stress under heat waves?" *Journal of Geophysical Research Atmospheres*, vol. 121, no. 10, pp. 65–78, 2017.

[38] M. Tewari, J. Yang, H. Kusaka, F. Salamanca, C. Watson, and L. Treinish, "Interaction of urban heat islands and heat waves under current and future climate conditions and their mitigation using green and cool roofs in New York City and Phoenix, Arizona," *Environmental Research Letters*, vol. 14, no. 3, p. 034002, 2019.

[39] P. Pratiman, S. Karmakar, and S. Ghosh, "Impact of green roofs on heavy rainfall in tropical, coastal urban area," *Environmental Research Letters*, vol. 16, no. 7, p. 074051, 2021.